Conformation of ATPMg(II) bound at the specific site on bovine serum albumin: ^{1}H-nuclear magnetic resonance study

Hari Pada Maity and Gotam K. Jarori*

Tata Institute of Fundamental Research, Homi Bhabha Road, Colaba, Mumbai 400 005, India

Bovine serum albumin (BSA) binds one molecule of adenosine 5′-triphosphate (ATP) at one of the fatty acid-binding sites. Interaction of ATPMg(II) with BSA and its conformation in the bound form has been investigated using ^{1}H-nuclear magnetic resonance (NMR). Binding of nucleotide with albumin results in downfield shift of all the ligand proton resonances, indicating the involvement of adenine as well as ribose moiety in binding interactions. Measurements of change in chemical shifts of H2, H8 and H1′ protons of the ATP in the bound form as a function of ligand concentration, has yielded a dissociation constant of K_d ~ 2 mM for ATPMg(II) with albumin. Two dimensional transferred nuclear Overhauser spectroscopy (TRNOESY) was used to determine the inter-proton distances in ATPMg(II) bound to BSA. In order to select a concentration range of the ligand where binding occurs exclusively at the specific site, we have measured the NOE intensities for H1′–H2′ protons as a function of ATP concentration. For determining the conformation of bound ATPMg(II) at the specific site, NOE intensities have been measured for several mixing times (τ_m = 40–200 ms). The resulting NOE buildup curves were analysed using complete relaxation matrix calculations to determine various inter-proton distances. Examination of amino-acid sequence of BSA has led to the identification of a region GVKGLSRS (aminoacyl residues 425–432) which is very similar to the consensus sequence present in several ATP-binding proteins. On the basis of observed similarities in the conformation of bound ATP with that of other ATP-utilizing enzymes and the presence of the nucleotide binding consensus sequence, we propose that the specific ATP binding site is located on Domain-III of BSA.

SERUM albumin is one of the most abundant non-glycosylated proteins in the blood plasma. It contributes about 80% of the colloidal osmotic pressure which provides the driving force to keep fluid within blood vessels[1,2]. The most unique feature of the albumin is its ability to bind a wide variety of biological materials. This includes divalent cations, a variety of metabolites, hormones, drugs, free fatty acids, etc.[1,3,4]. Several of these functions depend on the extraordinary ability of albumin to bind hydrophobic as well as hydrophilic compounds. Recent X-ray studies on human serum albumin complexed with different ligands have shown that the principal ligand binding sites were located in subdomains IIA and IIIA (ref. 5). Several aromatic compounds bind at these two sites. Their general orientation in the binding cavity depends upon the nature of substitutions in the aromatic ring.

In a recent study Bauer *et al.*[6] used a number of spin labelled derivatives of ATP and studied their binding to bovine serum albumin (BSA) using the electron spin resonance method. It was found that ATP binds at a specific site on BSA with a stoichiometry of 1 : 1 and a dissociation constant in the range of 50–100 μM. BSA is known to bind about 4–5 moles of fatty acids per mole of protein[7,8] and it is proposed that nucleotide interacts at one of these amphipathic regions on the surface of the protein[6]. ATP with an aromatic ring (adenine), a hydrophilic sugar moiety (ribose) and a highly charged triphosphoryl tail, appears to be an excellent probe to characterize the specific binding site on the albumin. With this in view, we have studied the interaction of ATPMg(II) with BSA using NMR. The ability of NMR to observe every ligand proton has allowed us to identify the regions of the ligand which are in direct contact with the protein in the protein–ligand complex. Further, the conformation of the bound nucleotide has been determined, using proton transferred nuclear Overhauser effect spectroscopy (TRNOESY)[9–11] in 2D-NOESY mode[12] and has been compared with those of other nucleotide-binding proteins[13–23].

Materials and methods

Materials

Bovine serum albumin was purchased from Armour Pharmaceutical Company. ATP, 4.9 M – $MgCl_2$ solution and D_2O (99.96 atom% D) were obtained from Sigma. Chelex-100 was supplied by Bio-Rad. Tris(hydroxymethyl)aminomethane-d_{11} (99.0 atom% D) (Tris-d_{11}) was purchased from ISOTEC Inc, USA. All other chemicals were of Analar grade and used without purification.

*For correspondence.

Sample preparation

Bovine serum albumin was dissolved in 20 mM sodium phosphate, pH 7.5, and dialysed against the same buffer. The solution was treated with Chelex-100 to remove trace metal ions. H_2O was exchanged with D_2O by dialysing the sample against 20 mM sodium phosphate, pH 7.5, (without any isotopic correction) in a dialysis cell. At least ten changes of buffer were made for solvent exchange. This was lyophilized once and then dissolved in 99.96% D_2O. The concentration of BSA was determined spectrophotometrically with A_{280} = 0.66 mg^{-1} ml cm^{-1} and molecular weight of 66,000 Daltons[24]. Nucleotide solution was also passed through Chelex-100 column, lyophilized and dissolved in D_2O. The concentration of ATP was determined using $A_{259} = 15.4\ mM^{-1}\ cm^{-1}$.

NMR measurements

^{1}H-NMR measurements were made on a Bruker-AMX500 NMR spectrometer. In all the measurements, sample temperature was maintained at 10°C. Chemical shifts were measured relative to the internal standard, sodium trimethylsilyl propionate-2,2,3,3-d_4 (TSP). 1D-^{1}H NMR spectra were recorded with 16 K data points, 6024 Hz spectral width, 2 s relaxation delay and 64 transients were averaged for each spectrum. NOESY time domain data were acquired with 256 t_1 increments and 2 K t_2 points in the phase sensitive mode with the use of TPPI[25]. Sixty-four scans were averaged for each t_1 increment. Measurements were made with mixing times 40, 80, 120, 160 and 200 ms. The carrier frequency was placed at the HDO resonance in all the experiments. The solvent resonance was suppressed by irradiation using the decoupler channel during intervals of relaxation delay, the t_1 period, and the mixing time. The acquisition parameters were, 1.5 s relaxation delay, 0.17 s acquisition time, and 6024 Hz sweep width.

Data were processed on an Aspect-X32 computer with Bruker software. All the data were processed identically with a two-dimensional Fourier transformation along both dimensions with a Gaussian apodization and a zero filling in t_1 to obtain 1 K (F1) × 2 K (F2) real data points. The spectra were phased to pure absorption mode. The volume of the cross peaks was determined by integration. Percentage of NOEs was derived by dividing the observed cross peak volume by the diagonal peak volume of H1′ extrapolated to zero mixing time and then multiplying it by 100. In experiments where measurements were made only for a single mixing time, the diagonal intensity of H1′ in the same spectrum was used to determine the per cent NOE.

Determination of binding constant

In an equilibrium between a macromolecule E and ligand L,

$$E + L \rightleftharpoons EL,$$

the dissociation constant is given by

$$K_d = [E][L]/[EL].$$

For a given value of K_d, E_T and L_T, where E_T and L_T are the total concentrations of the macromolecule and the ligand; the mole fraction of the bound ligand (P_M), i.e. $[EL]/[L_T]$ can be derived easily. Further, if the binding of L to E results in a change in chemical shift of L resonance by $\Delta\omega$, then under conditions of fast exchange it can easily be shown that

$$\Delta\omega = P_M \Delta\omega_M,$$

where $\Delta\omega_M$ is the chemical shift of the fully bound form of the ligand with respect to its position in unbound form[26]. Thus, the measurement of the change in the chemical shift where a fixed concentration of macromolecule is titrated with varying concentrations of the ligand, can be analysed by two parameter iterative fit to derive the values of K_d and $\Delta\omega_M$.

Relaxation matrix calculations

Simulations of complete NOE buildup curves in a TRNOESY experiment are greatly simplified if the fast exchange condition prevails[27], i.e. the 'on' and 'off' rates of the ligand must be faster than the typical cross relaxation rates[21,28]. In the limits of fast exchange, the intensity of the $i \leftarrow j$ cross peak represents a polarization transfer from spin j to i, for a mixing time τ_m and is given by[18,20,21]

$$m_{i \leftarrow j}(\tau_m) = (e^{-R\tau_m})_{ij} M_{oj} \quad (1)$$

$$= [1 - R\tau_m + \tfrac{1}{2} R^2\tau_m^2 - \tfrac{1}{6} R^3\tau_m^3 + \ldots]_{ij} M_{oj}, \quad (2)$$

where M_{oj} is the equilibrium value of the j spin magnetization and R is an average relaxation matrix given by

$$R = p_b W^b + p_f W^f, \quad (3)$$

where p_b and p_f are bound and free fractions of ligand each containing n-spins[27,29,30], W^b and W^f are the dipolar interaction[27,31–34] terms between two protons in bound and free form respectively and are given by

$$W_{ij} = W_{ji} = \frac{\gamma^4 \hbar^2 \tau_c}{10 r_{ij}^6} \left[-1 + \frac{6}{1 + 4\omega^2 \tau_c^2} \right] \quad (4)$$

and

$$W_{ii} = \frac{\gamma^4 \hbar^2 \tau_c}{10} \left[1 + \frac{3}{1 + \omega^2 \tau_c^2} \frac{6}{1 + 4\omega^2 \tau_c^2} \right] \sum_{k \neq i} r_{ik}^{-6}, \quad (5)$$

in which γ and ω are the gyromagnetic ratio and Larmor frequency of the protons, r_{ij} is the distance between spins i and j, and τ_c is the isotropic rotational correlation time. Equations (4) and (5) assume that the spin system is in a single conformation characterized by distance r_{ij}, and undergoing isotropic rotational diffusion characterized by the τ_c. Equation (2) shows that, for short mixing times, the build-up of the intensity of a cross peak in a TRNOESY spectrum, given by $m_{i \leftarrow j}(\tau_m)$ vs τ_m, is a polynomial in τ_m, and the initial slope of the build-up which is just the linear term, yields R_{ij}. Since usually $\tau_c^b > \tau_c^f$, p_b/p_f is 0.1–0.15, the last term in equation (3) is negligible so that

$$R_{ij} = P_b W_{ij}^b. \quad (6)$$

From equations (4) and (5) it can easily be shown that the ratio of initial slopes for different spin pairs is related to the corresponding internuclear distances in the bound conformation as

$$(R_{ij}/R_{ik}) = (r_{ik}^b/r_{ij}^b)^6. \quad (7)$$

Here $r_{ij}^b = 2.90 \pm 0.2$ Å is the calibration distance between H1′ and H2′. This distance is known to be independent of the nucleotide conformation[15,35]. The inter-proton distances derived using equation (7) were used as initial distances and a comprehensive analysis of data was done using equations (1) and (2) to obtain an iterative fit between theory and experiment.

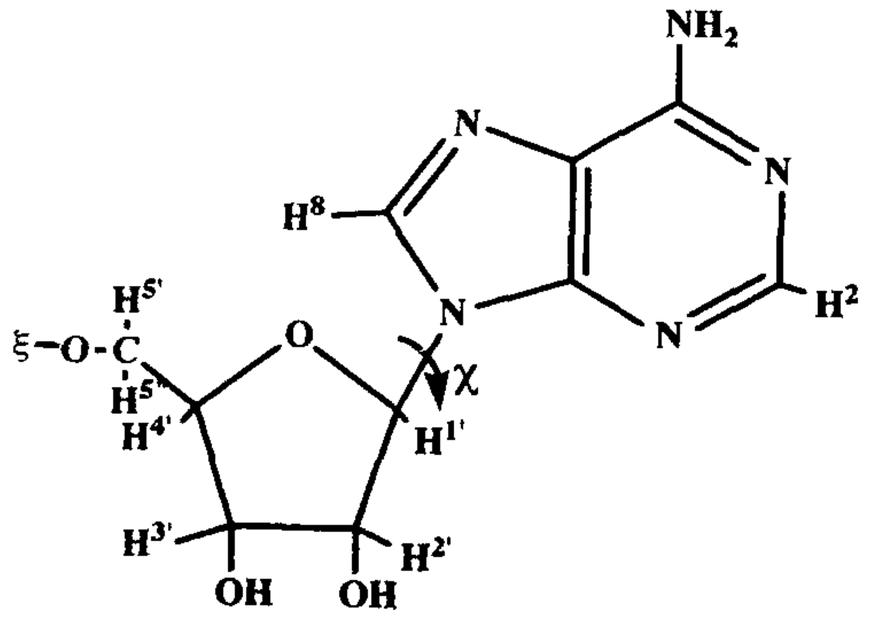

Figure 1. Schematic diagram of adenosine moiety of ATP, indicating the proton numbering system used here.

Energy minimization and molecular modelling

Molecular modelling and restrained energy minimization were performed using Insight II (V2.3.0) in the software package, Discover (V2.9.5) supplied by Biosym Technologies. The software was run on Iris Indigo work station supplied by Silicon graphics computer systems. The calculations were performed on adenosine molecule in vacuum. The inter-proton distances derived after complete relaxation matrix calculations were used as restraints allowing ±10% variation in the distance. The energy was minimized using steepest descent method followed by conjugate gradients method available with the software package.

Results and analysis

Binding of ATPMg(II)

In ^{1}H-NMR spectrum of ATPMg(II), resonances due to H2, H8, H1′ (see Figure 1 for nomenclature of various protons in ATP) are observable at 8.51, 8.22 and 6.14 ppm respectively. Binding of ATPMg(II) to BSA results in downfield shift of all the three resonances. The H2 proton resonance of adenine ring exhibits the largest shift. A sample containing 0.50 mM BSA in 25 mM Tris-d_{11}-Cl, pH 7.5, and 25 mM $MgCl_2$, was titrated with ATP in the concentration range of 0.43–4.73 mM. The observed change in the chemical shift of a proton was measured in Hz, from the corresponding resonance of ATPMg(II) in the absence of BSA. Largest downfield shift was observable at the lowest concentration of ATP. With increasing concentration of ATP, the resonances tend to shift towards the unbound ATP positions. Such behaviour is characteristic of a fast exchange condition where the rate of exchange of a ligand between bound and free environment is faster than that of the difference in chemical shift in two states. The data from this experiment have been analysed (as described above) to determine the dissociation constant for ligand binding (K_d) and the change in chemical shift for various protons in the bound form ($\Delta\omega_M$). Figure 2 presents the observed change in chemical shift measured from the respective free ligand resonance as a function of mole fraction of the bound ligand. The dissociation constant (K_d) derived for ATPMg(II) is 2.00 ± 0.15 mM. Downfield shift of H2, H8 and H1′ resonances in bound form with respect to free form are 191 ± 12 (0.382 ppm), 76 ± 6 (0.158 ppm), and 66 ± 5 (0.132 ppm) Hz respectively. In a simple case of two site exchange, if ω_A and ω_B are the resonance frequencies at the two sites (free and bound respectively) in the absence of exchange and τ_A and τ_B are the corresponding lifetimes at the two sites when exchange occurs, the fast exchange condition[36] can be defined by

$|\omega_A + \omega_B| = \Delta\omega_M < \tau_A^{-1}, \tau_B^{-1}$. Since the τ_B is the lifetime of ligand in EL complex, τ_B^{-1} represents the rate of dissociation of ligand (k_{off}) from the complex. Thus, it can be shown that under fast exchange condition, $\tau_B^{-1}(k_{off}) > \Delta\omega_M$ $(2\pi\Delta\nu)$. The largest change in chemical shift of H2-proton in the bound form allows us to set the lower limit for the rate of dissociation of ligand from the complex (k_{off}), that is $k_{off} \gg 1200\,s^{-1}$.

Dependence of NOE on ligand concentration

Figure 3 presents a typical NOESY spectrum of BSA. ATPMg(II), where several ligand inter-proton NOEs are observable as off diagonal peaks. To observe the site-specific NOEs arising due to interaction of ligand at the site of interest, appropriate sample conditions must be determined[18]. We have measured TRNOESY spectra with a mixing time of 120 ms at several different concentrations of the ligand. In each case the ratio of protein to ligand was maintained at 1 : 10. Note that protein concentration will also vary along with the ligand. Separate samples were prepared for each ATP concentration to avoid errors due to dilution. Figure 4 shows a plot of per cent NOE for H′–H2′ (distance between these two protons is invariant, irrespective of the nucleotide conformation) as a function of ATP concentration. Initial increase in per cent NOE to ~2% for a ligand concentration of 5 mM is indicative of gradual saturation of specific nucleotide-binding site. Observed increase in per cent NOE at ligand concentrations > 5 mM may arise due to weak binding of ATPMg(II) at some adventitious site(s). Similar behaviour has been observed in case of rabbit muscle creatine kinase[18] and yeast pyruvate kinase[20]. From these data it is clear that for the determination of bound nucleotide conformation, measurements must be performed on a sample with a ligand concentration < 5 mM.

Structure-dependent intramolecular NOE measurements

For the determination of conformation of adenosine moiety bound to BSA, measurements were made on a sample containing 4.0 mM ATP. Such sample composition maximizes the binding of ligand at the specific site and restricts interaction at low affinity non-specific sites.

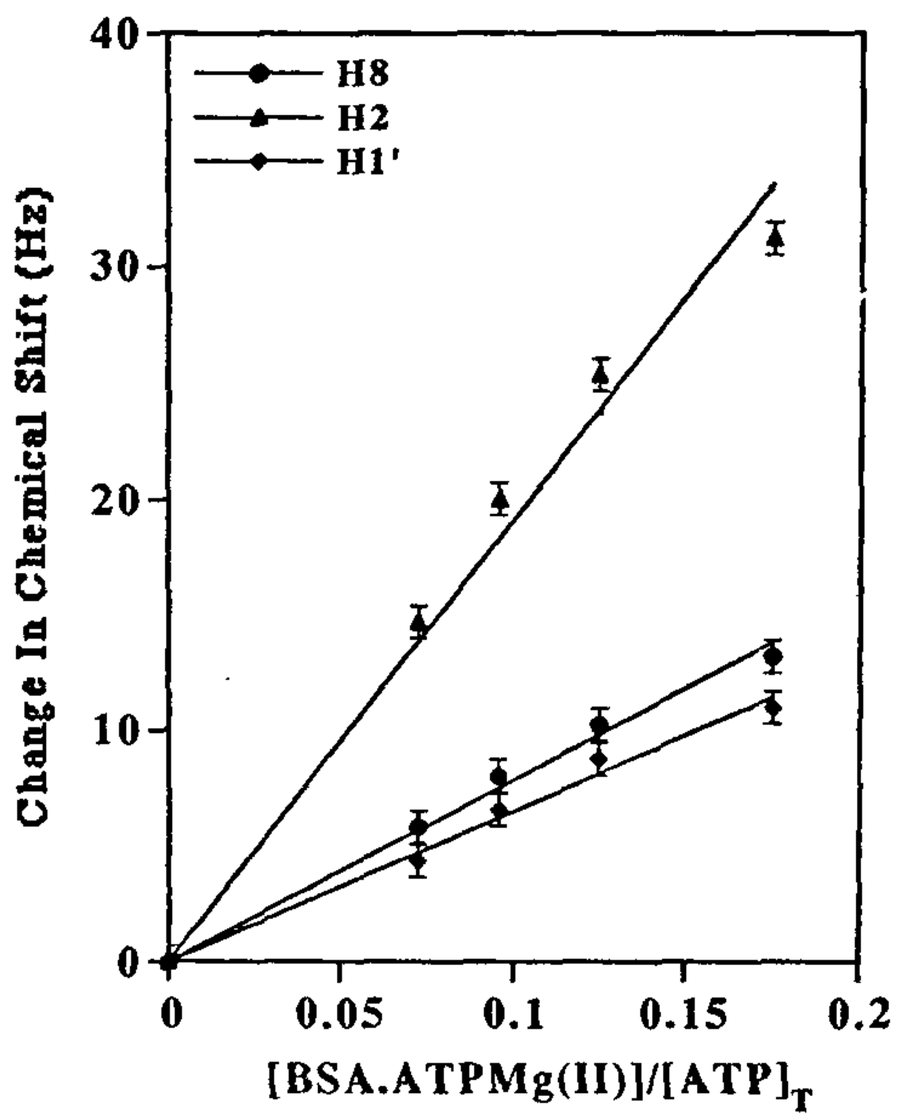

Figure 2. A plot of observed downfield change in chemical shift (Hz) of H2, H8 and H1′ protons of ATP measured from the respective free resonances, as a function of bound ATP mole fraction ($[BSA.ATPMg(II)]/[ATP]_T$). Sample contained 0.50 mM BSA; 20 mM $MgCl_2$; 25 mM Tris-(d_{11})-HCl pH 7.5 and the ATP concentration was varied from 0.43 to 4.73 mM. The spectra were recorded at 500 MHz, 10°C with a digital resolution of 0.35 Hz. The points are experimental and the solid curves are computed with a $K_d = 2.0$ mM for BSA.ATPMg(II) complex and the difference in chemical shift for bound and free resonances to be 191 ± 12, 76 ± 6 and 66 ± 5 Hz for H2, H8 and H1′ protons respectively.

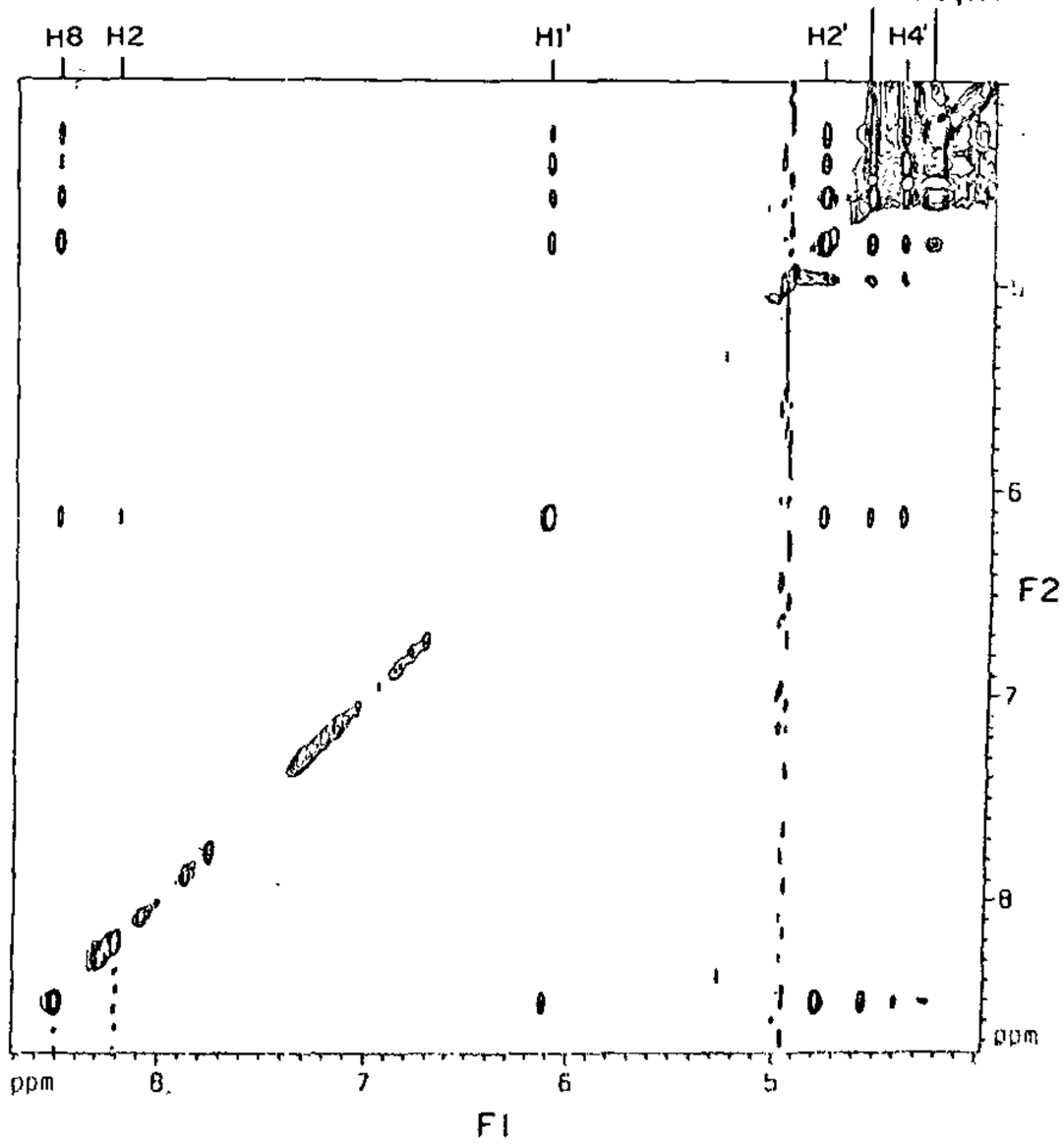

Figure 3. TRNOESY spectrum of BSA.ATPMg(II) complex recorded at 500 MHz and 10°C. The sample contained 0.572 mM BSA; 4.0 mM ATP; 20 mM $MgCl_2$ in 20 mM sodium phosphate, pH 7.5. The sample volume was 600 µl. NOESY time domain data were collected with $256 \times t_1$ increments and 2 K points during each accumulation in t_2. The mixing time of 160 ms and a relaxation delay of 2 s were used for the spectrum presented here. Two-dimensional Fourier transformation was performed along both the dimensions with a Gaussian apodization and zero-filling to obtain 1 K (F1) × 2 K (F2) data set. The spectra were phased to pure absorption phase.

The mole fraction of bound ligand (P_b) was also within the range (~ 0.1–0.25) as suggested by Campbell and Sykes[30,37] on the basis of theoretical considerations. The final sample composition chosen for NOE measurements was 0.572 mM BSA, 4.0 mM ATP and 20 mM $MgCl_2$ in 20 mM sodium phosphate, pH 7.5. Under such sample condition and for a $K_d = 2$ mM, P_b is ~ 0.1. The experimentally measured NOE buildup curves are shown in Figure 5, where per cent NOE is plotted as a function of mixing time for different proton pairs. The points represent experimentally measured values, while the solid curves were theoretically simulated as described below.

NOE buildup curves (shown in Figure 5) were analysed to obtain the inter-proton distances. The data analysis was performed in a similar way as was done for creatine kinase and arginine kinase[18,19]. Initially, the experimental NOEs were fitted with a second order polynomial in τ_M, including (0, 0) point as a part of data. Two distinct resonances are observed for H5′ and H5″ of free ATP. However, in the presence of Mg(II), these two resonances overlap. In the analysis of data here, these two protons were treated as a single proton and observed cross peak intensities involving H5′ and H5″ were divided by a factor of two before fitting them with the polynomial. Using a calibration distance of 2.9 Å for H1′H2′ (refs 15, 20) in conjunction with equation (7) and the initial slopes obtained for different proton-pairs, a set of inter-proton distances were determined. NOE data for H1′–H2′ with the calibration distance of 2.9 Å, also yields a value of $P_b\tau_c^b$ [see equations (4) and (6)]. These two parameters were separated by determining the P_b from the known dissociation constant. The set of initial slope distances, P_b and τ_c^b, obtained in this manner were used as a starter for complete relaxation matrix calculations. The cross peak intensities were calculated for each spin pair as a function of mixing time (τ_m) according to equations (1), (3) and (4). To account for the contribution of free ATPMg(II) [see equation (3)], a τ_c^f of 0.3 ns (ref. 38) and inter-proton distances from an energy minimized structure were used. To obtain a better fit for the data at larger mixing times, a leakage term was added to account for the contributions arising from any external relaxation mechanism (see legend to Figure 5). The buildup curves computed theoretically on the basis of these parameters were then compared with the experimental data. At this stage any of the parameters, i.e. τ_c^b, r_{ij} and leakage terms could be adjusted to obtain the best fit for the experimental data. The bound correlation time, τ_c^b, chosen for the best fit of experimental data was 53 ns. The inter-proton distances determined from the analysis of TRNOE data are given in Table 1 along with the initial slope distances. The solid curves were computed using this set of distances along with other parameters mentioned in the legend of Figure 5. The distances derived from initial slope approximation and relaxation matrix calculations are plotted in Figure 6 *a*. It is interesting to note that initial slope approximation underestimates the inter-proton distances which are > 3.5 Å. However, distance < 3.5 Å shows a good agreement between the two methods.

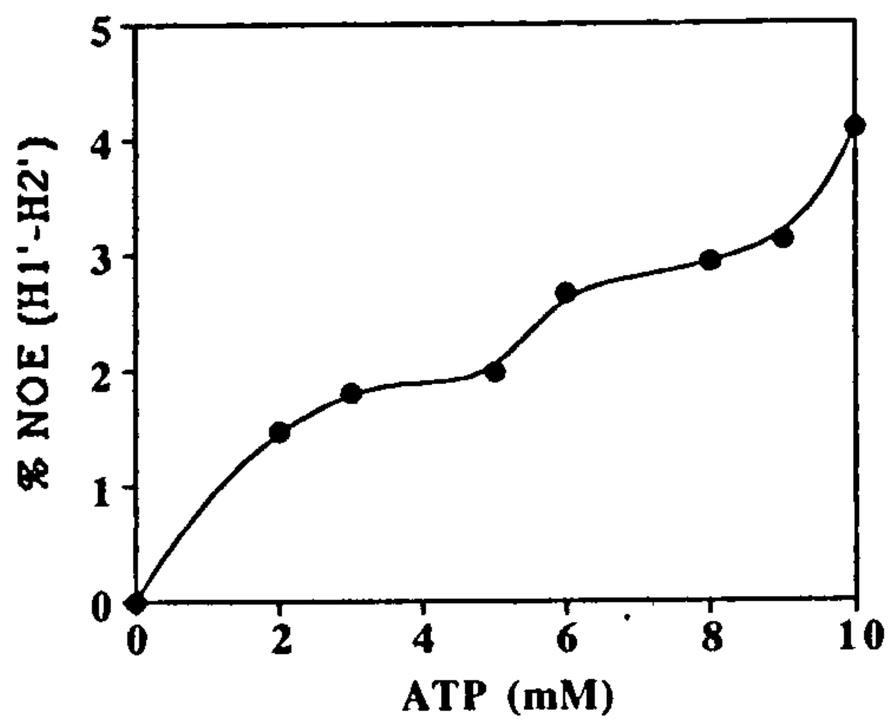

Figure 4. Concentration dependence of per cent NOE for H1′–H2′ proton pair in BSA.ATPMg(II) complex for a mixing time of 120 ms. The ATP concentration was varied between 2 and 10 mM. The ATP : BSA ratio was kept at 10 : 1. The sample contained 2–10 mM ATP; 0.2–1 mM BSA; 20 mM $MgCl_2$ in 20 mM sodium phosphate, pH 7.5. The experimental points are represented by circles and the solid curves represent smooth interpolation through the experimental points.

Bound nucleotide structure

The inter-proton distances derived from analysis of NOE data (see Table 1) were used as restraints in energy minimization calculations using Discover (V2.9.5) in conjunction with Insight II (V2.3.0). During minimization, experimentally obtained distances were used as target distances and a variation of ± 10% was allowed. A symmetrical simple harmonic function with a force constant of 50 kcal mol^{-1} $Å^{-2}$ was used to restrain the inter-atomic distances within the range. Since there were no distances determined in the triphosphate chain region of ATP, calculations were performed only on adenosine molecule. Distance restraints were applied sequentially[21], starting with H8 and all other protons. In the second step, the distances between H1′ and all other protons were used. In the third and the final step, all the distances were used. Each time, the energy minimization was performed using conjugate gradient method. The initial structure obtained in this manner fitted well with target distances. However, the energy of such structure was quite high compared to the energy of the free adenosine molecule. To further refine the initial structure, all the distances were used but the force constant was reduced to 25 kcal mol^{-1} $Å^{-2}$. This resulted in a structure with significantly lower energy with minor changes in inter-proton distances. Inter-proton distances between

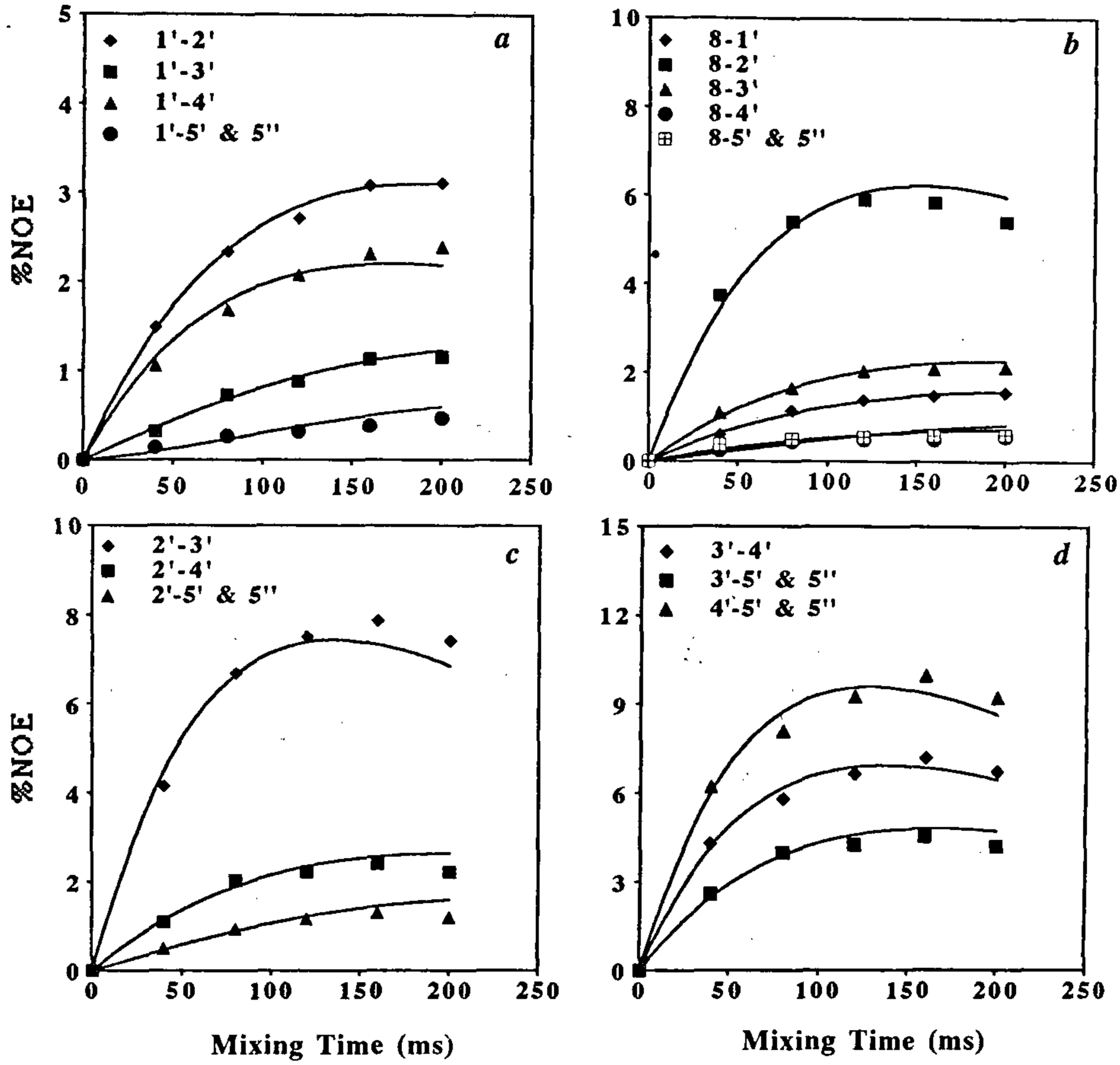

Figure 5. Per cent NOE for different pairs of ATP protons as a function of mixing time for BSA.ATPMg(II) complex. 600 µl of the sample containing 0.572 mM BSA, 4.0 mM ATP, 20 mM $MgCl_2$ in 20 mM sodium phosphate, pH 7.5 was used. Spectral acquisition and processing parameters are described in 'Materials and methods'. The points represent experimentally measured cross peak volumes and the solid curves are the simulations based on the relaxation matrix distances given in Table 1. External relaxation rates for H8, H2, H1′, H2′, H3′, H4′, H5′ and H5″ used in the fitting routine are 4.6, 2.0, 3.33, 3.33, 3.33, 2.86, 4.0 and 4.0 s^{-1} respectively. The rotational correlation time used for the bound ligand is 53 ns.

various pairs of protons in energy minimized structure are listed in Table 1. There are three violations in upper bound (between proton pairs H2′–H4′, H2′–H5′ and H3′–H5′) and two in lower bound distances (between proton pairs H2′–H3′ and H1′–H5′) (see Figure 6 *b*). Note that in these five violations, three involve H5′ whose distance from other protons is difficult to determine accurately. The sum of upper bound violations (SUV) is 1.03 Å and sum of lower bound violations (SLV) is 0.14 Å. Thus the distances in energy minimized structure match reasonably well with those determined by NOEs. The structure of the nucleotide bound to BSA derived above is schematically represented in Figure 7. It has a glycosidic torsion angle $\chi = 48 \pm 5°$, indicating an *anti* configuration of the adenine ring with respect to ribose. The values of various dihedral angles for the sugar ring are given in Table 2. In the notation of Altona and Sunderalingam[39], the phase angle of pseudorotation is about 150° corresponding to an unsymmetrical C2′-endo-C1′-exo twist ($^2T_1$) sugar pucker. The amplitude of the sugar pucker, τ is about 16°.

Discussion

Binding of ATP to BSA at a specific site was first reported by Bauer *et al.*[6]. Using appropriate spin labelled nucleotide analogues, these authors determined the binding constant for ATP to be in the range of 50–100 µM. Competitive displacement of bound spin probes by stearic acid suggested that the nucleotide binds at the site where the fatty acids interact. BSA is known to have about five fatty acid sites[7], with a binding constant ~ 10^6–10^8 M^{-1}. Differential nature of these sites is evident

Table I. Inter-proton distances determined for ATPMg(II) bound to bovine serum albumin. The uncertainty in distances is about ± 0.20 Å. Also note that distances of H5′ and H5″ from any other proton are not determined separately as both protons resonate at the same frequency. Only in restrained energy minimization, this differentiation is made and separate distances are obtained

Proton pair	Inter-proton distances (Å)		
	Initial slope	Relaxation matrix	Energy minimized
H8–H1′	3.29	3.37	3.66
H8–H2′	2.49	2.50	2.36
H8–H3′	3.05	3.12	3.38
H8–H4′	3.86	4.35	4.11
H8–H5′	3.73	3.90	3.70
H8–H5″	3.73	3.90	4.12
H1′–H2′	2.90	2.90	2.93
H1′–H3′	3.59	3.80	4.00
H1′–H4′	3.06	3.00	3.23
H1′–H5′	4.29	5.50	4.86
H1′–H5″	4.29	5.50	5.19
H2′–H3′	2.42	2.37	2.08
H2′–H4′	2.96	3.05	3.58
H2′–H5′	3.36	3.66	4.39
H2′–H5″	3.36	3.66	4.05
H3′–H4′	2.46	2.40	2.67
H3′–H5′	2.66	2.65	3.36
H3′–H5″	2.66	2.65	2.35
H4′–H5′	2.32	2.25	2.49
H4′–H5″	2.32	2.25	2.51

from the fact that ethanol binds only at three of these sites. Ethanol binding fatty acid sites appear to be the same where 1-anillino-8-napthalenesulfonate (1,8-ANS) also interacts[24,40,41]. Further differences in binding determinants at these fatty acid sites are evident from the fact that ATP binds at only one of these sites. This region on the surface of BSA is likely to be amphipathic, i.e. aminoacyl residues present at this site are likely to be apolar and cationic. In the experiments presented here, we have determined the dissociation constant for binding of ATPMg(II) with BSA which is about an order of magnitude larger than that of free ATP (ref. 6). At pH > 7, free ATP has four negative charges whereas ATPMg(II) complex has only two. Adenosine 5′-monophosphate (AMP), which has two negative charges (resembles ATPMg(II) in this respect), also binds weakly with a dissociation constant in the millimolar range[6]. Binding affinity of a ligand to fatty acid binding region of BSA seems to be critically dependent on the number of negative charges on the ligand molecule. The observation of significant changes in the chemical shifts (see Figure 2) of the adenine and the ribose ring protons, indicate that these two rings along with triphosphate chain are involved in direct interaction with the BSA. Although binding of nucleotide to BSA has no known physiological function, interaction of all three regions of ATP with protein suggests that binding domain may resemble other ATP utilizing proteins. We examined the amino-acid sequence of BSA for the presence of a consensus sequence found in several ATP-binding proteins[42]. Aminoacyl residues 425–432, which have a sequence GVKGLSRS, is very similar to ATP-binding consensus sequence. This sequence is part of Domain-III which is known to have one high affinity fatty acid-binding site[43]. It is quite likely that the specific ATP-binding site is located in Domain-III of the BSA.

In the titration experiment where chemical shifts of ATP protons were measured, we observe that at low

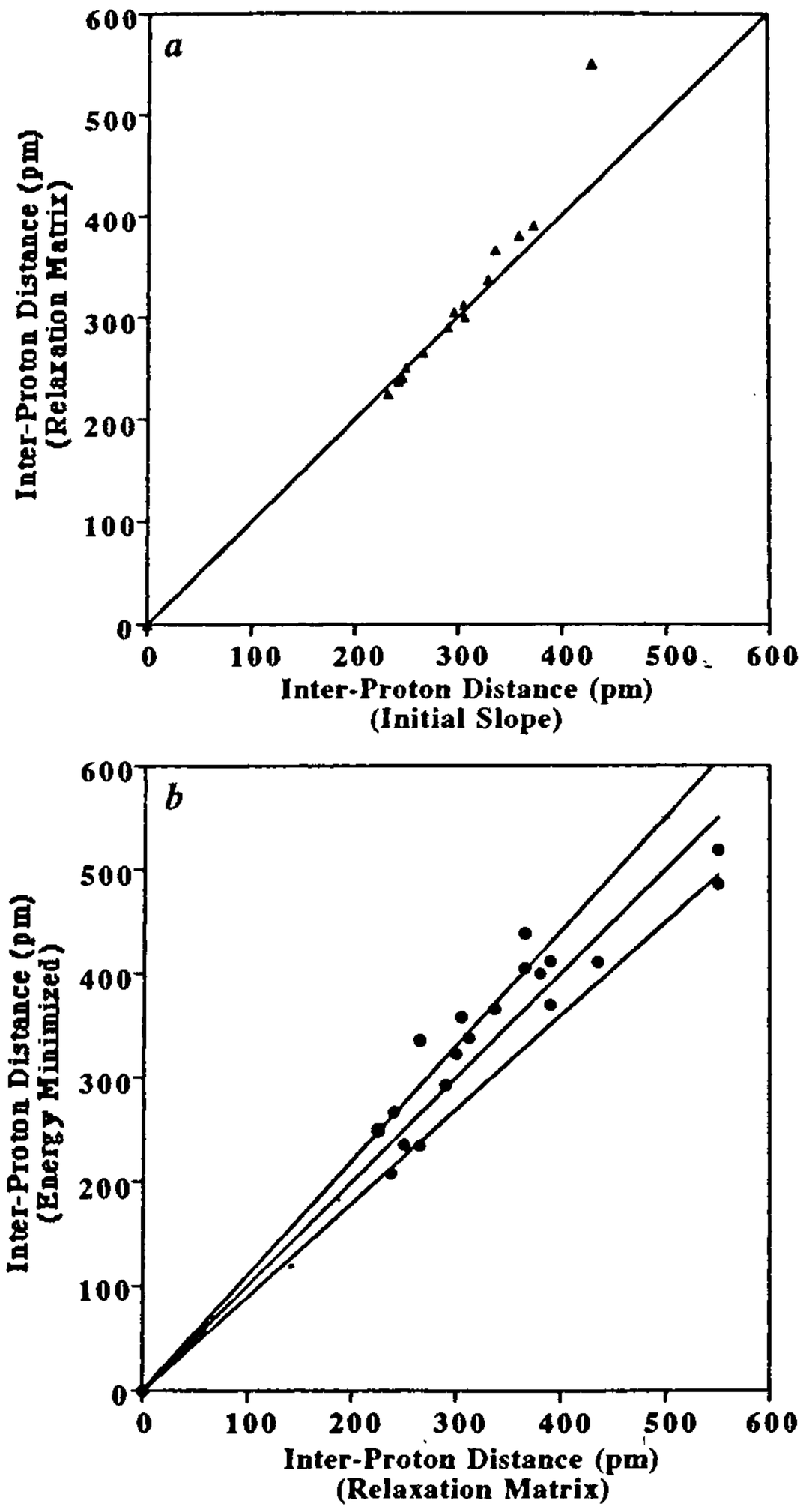

Figure 6. *a*, Comparison of inter-proton distances determined by initial slope approximation and complete relaxation matrix calculations. Fourteen different inter-proton distances determined for ATP in BSA.ATPMg(II) complex are presented. *b*, Comparison of relaxation matrix distances with the model distances derived from the final energy minimized structure of the bound nucleotide.

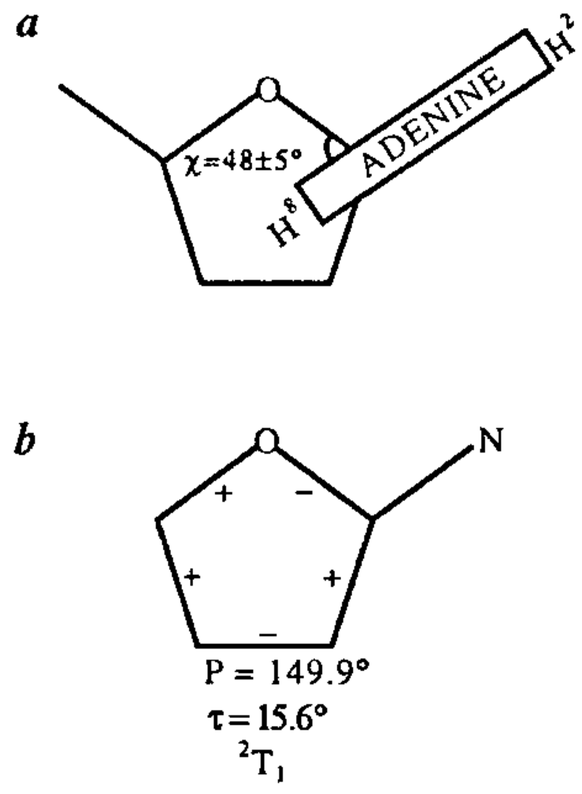

Figure 7. Schematic representation of ATPMg(II) structure bound at the specific site on the BSA (*a*) the glycosidic torsion angle (χ) and (*b*) the sign of various torsion angles defining the ribose conformation as well as the phase angle of pseudorotation (p) is mentioned.

Table 2. Different torsion angles and phase angle of pseudorotation (p) for the ribose when bound at the specific site on bovine serum albumin*

Torsion	Angle (degree)
χ (O4′–C1′–N9–C8)	48.0
ν_0 (C4′–O4′–C1′–C2′)	–11.6
ν_1 (O4′–C1′–C2′–C3′)	15.9
ν_2 (C1′–C2′–C3′–C4′)	–13.5
ν_3 (C2′–C3′–C4′–O4′)	6.6
ν_4 (C3′–C4′–O4′–C1′)	3.3
γ (O5′–C5′–C4′–C3′)	68.0
$p = \tan^{-1} \dfrac{(\nu_4 + \nu_1) - (\nu_3 + \nu_0)}{2\nu_2(\sin 36° + \sin 72°)}$	149.9**
$\tau = \dfrac{\nu_2}{\cos} p$	15.6

*The definition used for various torsion angles is the same as that described by Sanger[46].
**Since ν_2 is negative, 180° was added to the p value computed[39].

ligand concentration all proton resonances are shifted downfield to different extents. With increasing ligand concentration, the resonances shift progressively, approaching the chemical shift of free ligand at high ligand concentrations. Such behaviour is characteristic of a ligand resonance being in fast exchange[28]. The largest chemical shift change observed for H2 proton of adenine ring allows us to determine the upper limit for the inverse of life time of BSA. ATPMg(II) complex, i.e. $k_{off} >> 1200\ s^{-1}$. Decrease in binding constant with decreasing negative charges on triphosphoryl chain and observation of downfield shift of proton resonances of adenine and ribose ring suggest that all three regions of nucleotide are involved in binding interactions with the BSA.

The measurement of TRNOE between the H1′–H2′ proton pair of ATPMg(II) as a function of ligand concentration (Figure 4) shows that at the higher concentration of ligand, large contributions to observed NOE may arise due to binding at adventitious site(s). In this respect BSA behaves similar to creatine kinase[18] and pyruvate kinase[20]. Experimental evaluation of the extent of non-specific binding is essential for selection of proper sample composition where site-specific TRNOE measurements could be made. Theoretical analysis of TRNOE data collected under appropriate sample conditions (to maximize specific site binding) implicitly involve the following assumptions. Firstly, the fast exchange conditions prevail, i.e. the inverse of the life time of the ligand in the macromolecular complex should be larger than the typical proton–proton cross relaxation rates. Secondly, it is assumed that all proton pairs have a single effective rotational correlation time (τ_c^b). It is, therefore quite instructive to estimate relaxation rates and compare with the 'off' rate for ATPMg(II) from the protein complex. The 'off' rate for bound ATPMg(II) obtained for BSA. ATPMg(II) complex from chemical shift measurements is $>> 1200\ s^{-1}$. Bovine serum albumin, having a molecular weight of 66000 Daltons, may have a rotational correlation time as large as 60–70 ns. The cross relaxation rate between the two protons is given by $\gamma^4\hbar^2\tau_c/10\ r^6$ [see equation (4)]. For an inter-proton distance of 1.90 Å and $\tau_c = 70$ ns, the cross-relaxation rate is $85\ s^{-1}$. The cross-relaxation rate computed here is much less than the 'off rate' (k_{off}) of the ligand from the protein complex. Thus, our analysis of TRNOE data using the formulation evolved for fast exchange condition is valid. Further, use of a single rotational correlation time, $\tau_c^b = 53$ ns for all the proton pairs is justified by the fact that the binding of nucleotide with protein involves all three regions of ATP. This will rule out any differential segmental motion for the ligand. The correlation time, $\tau_c^b = 53$ ns which gives the best fit for the experimental data, is in close agreement with the value computed on the basis of Stokes equation (~ 60–70 ns). In most of the ATP utilizing enzymes, τ_c^b obtained from the analysis of TRNOE data are much smaller (by a factor of 2–10) compared to Stokes equation estimates[18–21,44,45] and this has been attributed to unaccounted spin diffusion in bound complexes.

The final structure determined for ATPMg(II) bound to BSA has a glycosidic torsion angle $\chi = 48 \pm 5°$. This value is in general agreement with that obtained for several ATP-utilizing enzymes, viz. creatine kinase ($\chi = 51 \pm 5°$)[18], arginine kinase ($\chi = 50 \pm 5°$)[19], pyruvate kinase (active site $\chi = 44 \pm 5°$, ancillary site $\chi = 46 \pm 5°$)[20], phosphoribosyl pyrophosphate synthetase ($\chi = 50 \pm 5°$)[21], Mut T ($\chi = 53 \pm 9°$)[23] (for AMPCPP). The sugar pucker, which is described by the phase angle of pseudorotation, $p = 149.9°$, determined here is unsymmetrical C2′-endo-

C1′-exo twist ($^2T_1$). The value of p differs greatly for different enzymes, e.g. 42.4° for pyruvate kinase (active site), 70.5° for creatine kinase, 114.9° for phosphoribosyl pyrophosphate synthetase, 130.8° for arginine kinase. Although the binding of ATPMg(II) to BSA has no known physiological function, it is interesting to note that the bound nucleotide has a conformation very similar to that at the active site(s) of several ATP-utilizing enzymes.

1. Peters, Jr., T., in *Advances in Protein Chemistry* (eds Anifinsen, Edsall and Richards), Academic Press, London, 1985, vol. 37, pp. 161–236.
2. Spector, A. A., in *Biochemistry and Biology of Plasma Lipoproteins* (eds. Scanu, A. M. and Spector, A. A.), Marcel and Dekker, New York, 1986, pp. 247–279.
3. Havel, R. J., Ekelund, L.-G. and Holmgren, A., *J. Lipid Res.*, 1967, **8**, 366–373.
4. Pederesen, A. O., Mensberg, K.-L. D. and Kragh-Hansen, U., *Eur. J. Biochem.*, 1995, **233**, 395–405.
5. He, X. M. and Carter, D. C., *Nature*, 1992, **358**, 209–215.
6. Bauer, M., Baumann, J. and Trommer, W. E., *FEBS Lett.*, 1992, **313**, 288–290.
7. Sklar, L. A., Hudson, B. S. and Simoni, R. D., *Biochemistry*, 1977, **23**, 5100–5108.
8. Perkin, R. C., Abumrad, N., Beth, A. H., Dalton, L. R., Park, J. H. and Park, C. R., *Biochemistry*, 1982, **21**, 4059–4064.
9. Albrand, P. L., Birdsall, B., Feeney, J., Roberts, G. C. K. and Burgen, A. S., *Int. J. Biol. Macromol.*, 1979, **1**, 37–41.
10. Clore, G. M. and Gronenborn, A. M., *J. Magn. Reson.*, 1982, **48**, 402–417.
11. Clore, G. M. and Gronenborn, A. M., *J. Magn. Reson.*, 1983, **53**, 423–442.
12. Anil Kumar, Ernst, R. R. and Wuthrich, K., *Biochem. Biophys. Res. Commun.*, 1980, **95**, 1–6.
13. Vasak, M., Nagayama, K., Wuthrich, K., Mertens, M. L. and Kagi, J. H. R., *Biochemistry*, 1979, **18**, 5050–5055.
14. Rosevear, P. R., Desmeules, P., Kenyon, G. L. and Mildvan, A. S., *Biochemistry*, 1981, **20**, 6155–6164.
15. Rosevear, P. R., Bramson, H. N., O'Brian, C., Kasier, E. T. and Mildvan, A. S., *Biochemistry*, 1983, **22**, 3439–3447.
16. Rosevear, P. R., Powers, V. M., Dowhan, D., Mildvan, A. S. and Kenyon, G., *Biochemistry*, 1987, **26**, 5338–5344.
17. Banerjee, A., Levy, H. R., Levy, G. C. and Chan, W. W. C., *Biochemistry*, 1985, **24**, 1593–1598.
18. Murali, N., Jarori, G. K., Landy, S. B. and Nageswara Rao, B. D., *Biochemistry*, 1993, **32**, 12941–12948.
19. Murali, N., Jarori, G. K. and Nageswara Rao, B. D., *Biochemistry*, 1994, **33**, 14227–14236.
20. Jarori, G. K., Murali, N. and Nageswara Rao, B. D., *Biochemistry*, 1994, **33**, 6784–6791.
21. Jarori, G. K., Murali, N. and Nageswara Rao, B. D., *Eur. J. Biochem.*, 1995, **230**, 517–524.
22. Seng, S., Velde, D. V., Gunn, C. W. and Himes, R. H., *Biochemistry*, 1994, **33**, 693–698.
23. Frick, D. N., Weber, D. J., Abeygunawardana, C., Giltis, A. G., Bessman, M. J. and Mildvan, A. S., *Biochemistry*, 1995, **34**, 5577–5586.
24. Daniel, E. and Weber, G., *Biochemistry*, 1966, **5**, 1893–1900.
25. Marian, D. and Wuthrich, K., *Biochem. Biophys. Res. Commun.*, 1983, **113**, 967–974.
26. Dwek, R. A., in *Nuclear Magnetic Resonance in Biochemistry*, Clarendon Press, Oxford, 1973, pp. 136–137.
27. Landy, S. B. and Nageswara Rao, B. D., *J. Magn. Reson.*, 1989, **81**, 371–377.
28. Lian, L. Y., Barsukov, I. L., Sutcliffe, M. J., Sze, K. H. and Roberts, G. C. K., *Methods Enzymol.*, 1994, **239**, 657–700.
29. Koning, T. M. G., Boelens, R. and Kaptien, R., *J. Magn. Reson.*, 1990, **90**, 111–123.
30. Campbell, A. P. and Sykes, B. D., *J. Magn. Reson.*, 1991, **93**, 77–92.
31. Abragam, A., *The Principles of Nuclear Magnetism*, Oxford University Press, London, 1961,
32. Noggle, J. H. and Schirmer, R. E., *The Nuclear Overhauser Effect*, Academic Press, New York, 1971.
33. Kalk, A. and Berendenson, H. J. C., *J. Magn. Reson.*, 1976, **24**, 343–366.
34. Keepers, J. W. and James, T. L., *J. Magn. Reson.*, 1984, **57**, 404–426.
35. Levitt, M. and Warshell, A., *J. Am. Chem. Soc.*, 1978, **100**, 2607–2613.
36. Pople, J. A., Schneider, W. G. and Bernstein, H. J., *High Resolution Nuclear Magnetic Resonance*, McGraw-Hill, New York, 1959, pp. 218–225.
37. Campbell, A. P. and Sykes, B. D., *Annu. Rev. Biophys. Biomol. Struct.*, 1993, **22**, 99–122.
38. Landy, S. B., Ray, B. D., Plateau, P., Lipkowitz, K. B. and Nageswara Rao, B. D., *Eur. J. Biochem.*, 1992, **205**, 59–69.
39. Altona, C. and Sunderalingam, M., *J. Am. Chem. Soc.*, 1972, **94**, 8205–8212.
40. Santos, E. C. and Spector, A. A., *Biochemistry*, 1972, **11**, 2299–2302.
41. Avdulov, N. A., Chochina, S. V., Daragan, V. A., Shroeder, F., Mayo, K. H. and Wood, W. G., *Biochemistry*, 1996, **35**, 340–347.
42. Fry, D. C., Kuby, S. A. and Mildvan, A. S., *Proc. Natl. Acad. Sci. USA*, 1986, **83**, 907–911.
43. Reed, R. G., Feldhoff, R. C., Clute, O. L. and Peters, T., Jr., *Biochemistry*, 1975, **14**, 4578–4583.
44. London, R. E., Perlman, M. E. and Davis, D. G., *J. Magn. Reson.*, 1992, **97**, 79–98.
45. Nirmala, N. R., Lippens, G. M. and Hallenga, K., *J. Magn. Reson.*, 1992, **100**, 25–42.
46. Sanger, W., in *Principles of Nucleic Acid Structure* (ed. Cantor, C. R.), Springer, New York, 1984, pp. 9–28.

ACKNOWLEDGEMENTS. We thank the National Facility for High Field NMR located at TIFR, Mumbai, for allowing us to make all the NMR measurements and use their graphics facility for molecular modelling. We thank Dr S. B. Landy of IUPUI, Indianapolis, USA for providing us with computer program for complete relaxation matrix calculations.

Received 26 September 1996; accepted 25 October 1996